Chinese Journal of Mechanical Engineering: Additive Manufacturing Frontiers 1 (2022) 100039

Contents lists available at ScienceDirect

Chinese Journal of Mechanical Engineering: Additive Manufacturing Frontiers

journal homepage: www.elsevier.com/locate/cjmeamf

A Review on Distortion and Residual Stress in Additive Manufacturing

Deqiao Xie[a], Fei Lv[b], Youwen Yang[c,*], Lida Shen[b], Zongjun Tian[b], Cijun Shuai[c], Bo Chen[d], Jianfeng Zhao[b,*]

[a] College of Energy and Power Engineering, Nanjing University of Aeronautics and Astronautics, Nanjing, 210016, China
[b] College of Mechanical and Electrical Engineering, Nanjing University of Aeronautics and Astronautics, Nanjing, 210016, China
[c] Institute of Bioadditive Manufacturing, Jiangxi University of Science and Technology, Nanchang, 330044, China
[d] School of Engineering, University of Leicester, Leicester, LE1 7RH, UK

ARTICLE INFO

Keywords:
Additive manufacturing
Distortion
Residual stress
Selective laser melting
Laser melting deposition

ABSTRACT

Additive manufacturing (AM) has gained extensive attention and tremendous research due to its advantages of fabricating complex-shaped parts without the need of casting mold. However, distortion is a known issue for many AM technologies, which decreases the precision of as-built parts. Like fusion welding, the local high-energy input generates residual stresses, which can adversely affect the fatigue performance of AM parts. To the best of the authors' knowledge, a comprehensive review does not exist regarding the distortion and residual stresses dedicated for AM, despite some work has explored the interrelationship between the two. The present review is aimed to fill in the identified knowledge gap, by first describing the evolution of distortion and residual stresses for a range of AM processes, and second assessing their influencing factors. This allows us to elucidate their formation mechanisms from both the micro- and macro-scales. Moreover, approaches which have been successfully adopted to mitigate both the distortion and residual stresses are reviewed. It is anticipated that this review paper opens many opportunities to increase the success rate of AM parts by improving the dimension precision and fatigue life.

1. Introduction

Additive manufacturing (AM), which is also known as 3D printing, is recognized as an emerging technology for the fields of aerospace, medical, and automobile [1–5]. It is an advanced processing technology, characterized by joining feedstock materials to make objects from three-dimensional model data, in a layer-by-layer fashion [6]. AM has already been adopted by the high-end automotive and aerospace industries due to its competitive advantages in terms of the fabrication of complex-shaped parts, high utilization rate of raw materials, short production cycle when compared with the casting [7–11]. In addition, AM broadens the freedom of design, which drives a design evolution in aerospace and art.

AM technologies are classified into seven groups including powder bed fusion, direct energy deposition, material extrusion, vat photopolymerization, sheet lamination, binder jetting and material jetting [11]. The former four processes have attracted much attention, based on the number of published work and AM applications in the market [12,13]. Powder bed fusion means that the powder bed is selectively melted or sintered by high-energy beam such as the laser and electron beam. It includes selective laser melting (SLM) [14–16], electron beam selective melting (EBSM) [17,18], and selective laser sintering (SLS) [19–21]. On the other hand, direct energy deposition is an AM process where the raw material (powder or wire) is directly melted and then deposited by laser, electron beam, and arc. It involves laser melting deposition (LMD) [22–25], electron beam free form fabrication (EBFFF) [26] or electron beam additive melting (EBAM) [27], and wire and arc AM (WAAM) [28–31]. Material extrusion means that rheologic raw material is extruded to create the part. Fused deposition modeling (FDM) [32,33] is a material extrusion process that uses heat source to drive the solid material into rheologic status. Vat photopolymerization is based on the mechanism of light curing, which includes stereo lithography appearance (SLA) [34,35] and digital light processing (DLP) [36–39].

Among the main AM technologies, the distortion and residual stresses are two frequently encountered and major obstacles that lower the dimension precision and performance of the built part. The deviation of the AM built part from its designed shape or dimension is termed as distortion [40]. It can occur when the built part is separated from the substrate or during the additive process [41], resulting in the decreased part's precision which is not easy to recover. If distortion occurs during the powder-bed-fusion AM, the distorted part can hinder the movement of roller, causing the building process broken down. Tensile residual stress is regarded as a threat to the part's mechanical properties, especially the fatigue performance. In the worst scenario, major cracks

* Corresponding authors.
E-mail addresses: yangyouwen@jxust.edu.cn (Y. Yang), zhaojf@nuaa.edu.cn (J. Zhao).

https://doi.org/10.1016/j.cjmeam.2022.100039
Received 21 October 2021; Received in revised form 13 March 2022; Accepted 15 March 2022
Available online 16 July 2022

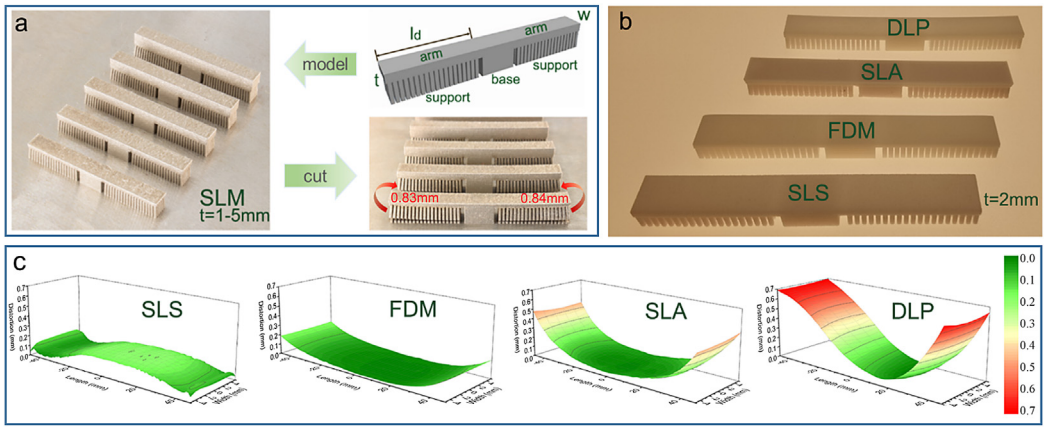

Fig. 1. Distortion of cantilever structures in AM: (a) Distortion of a cantilever structure built by SLM; (b) Cantilever structures (arm thickness $t = 2$ mm) built by SLS, FDM, SLA, and DLP; (c) Distortion pattern of the cantilever structures (arm thickness $t = 2$ mm) as shown in (b), measured by CMM [56].

can be developed during the AM process due to the large tensile stress [42].

The long history of thermal-cycle, multiple processing parameters, and complex structures lead to complex variations of distortion and residual stress. There have been several review articles concerning the residual stress related to AM [43–45]. However, the AM part distortion phenomenon has not been reviewed, to the best of the authors' knowledge. In fact, the distortion and residual stress are closely related. Therefore, the present paper provides a review of the distortion and residual stress together, with the aim to clarify the mechanism of these two major issues in AM. The pattern, evolution, and influencing factors of distortion and residual stress are investigated, which is followed by elaborating their mechanisms. In the end, approaches for mitigating the risk of distortion of the AM built part and managing residual stresses are discussed.

2. Distortion in AM

2.1. The pattern of distortion

The techniques available for part distortion measurements include coordinate measuring machine (CMM) [46,47], laser displacement sensor (LDS) [48–52], and digital image correlation (DIC) [53,54]. Based on the measurement results, most AM built parts exhibited the same distortion pattern, i.e., far ends of the part bent along the build direction [54–59]. As illustrated in Fig. 1, the cantilever structures built by various AM techniques, including SLM, FDM, SLA, and DLP, were all characterized by the same distortion pattern, whereas the SLS built part exhibited a limited buckling distortion. Figs. 2(a) and 2(b) show that both the "horizontally" and "vertically" prism specimens built by SLM experienced a similar distortion pattern characterized by the far ends "peeling up" along the build direction. Figs. 2(c) and 2(d) demonstrate that the corners of substrate were wrapped the most, when six blocks were deposited by EBSM. Figs. 2(e) and 2(f) show that crack and distortion can be generated simultaneously in the process of LMD due to thermal stress.

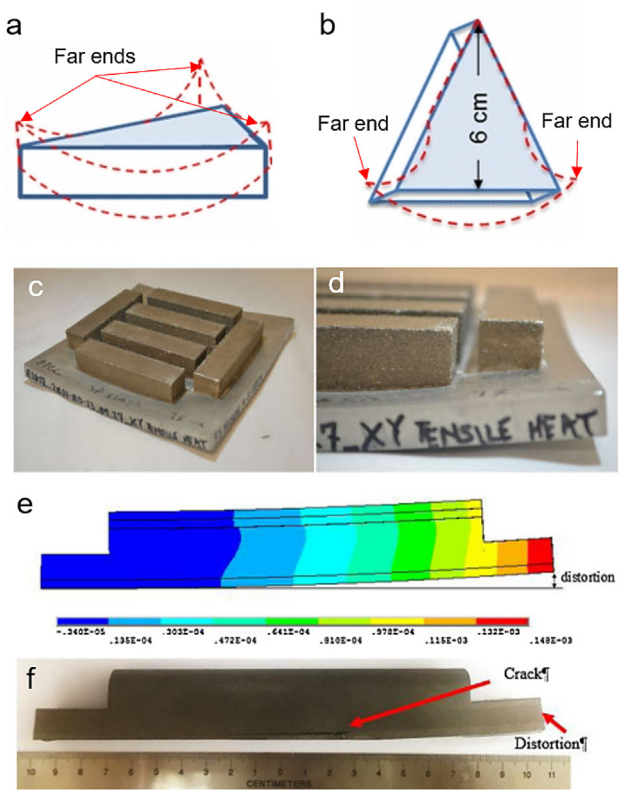

Fig. 2. Distortions of various specimens built by AM techniques: (a) "Horizontally" direction prism specimens built by SLM; (b) "Vertically" direction prism specimens built by SLM [54]; (c, d) Block specimens built by EBSM [57]; (e) Finite element simulation of a block specimen built by LMD [58]; (f) Experimental validation of a block specimen built by LMD [58].

2.2. The evolution of distortion

Studies have shown that the part may experience complex variations of distortion during the AM process [50,52]. Fig. 3 illustrates the distortion evolution during a typical cycle of the laser deposition process, i.e., the free end of substrate distorted downward during the deposition step (Fig. 3(b)), while it bent upward during the cooling step (Fig. 3(c)). Wen et al. [59] monitored the distortion behavior of the SLM process by using the strain gage. When the laser scanning started on the powder surface (Fig. 4(a)), the specimen bent upward significantly and instantaneously. After the laser scanning stopped, the specimen gradually recovered to its original position. Thereafter, the specimen continuously deformed after recovery and eventually showed a downward bent shape. When the laser scanning started on the specimen surface without the powder layer (shown in Fig. 4(b)), the initial compressive strain at the bottom was more significant than the condition of with the powder on top. After the laser scanning stopped, a much higher tensile residual strain was developed, followed by a relatively slower recovery during cooling. In the AM process, the free end of substrate exhibited a gradually increased

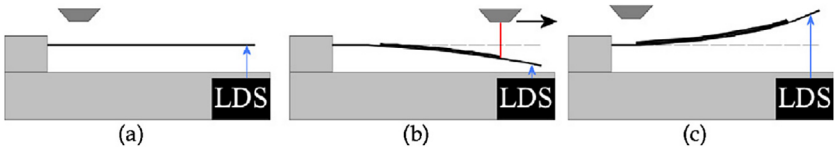

Fig. 3. Illustration showing distortion of the substrate during the laser deposition process: (a) Prior to deposition; (b) During deposition; and (c) During cooling (LDS means laser displacement sensor) [51].

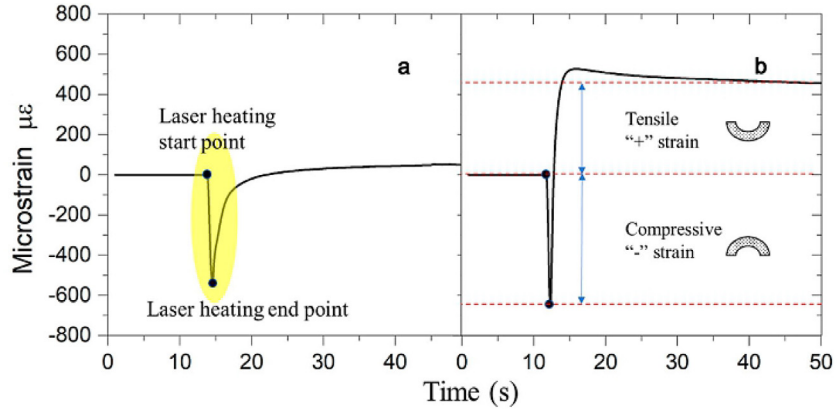

Fig. 4. (a) Distortion curve in single scanning with the powder layer; (b) Distortion curve in single scanning without the powder layer [59].

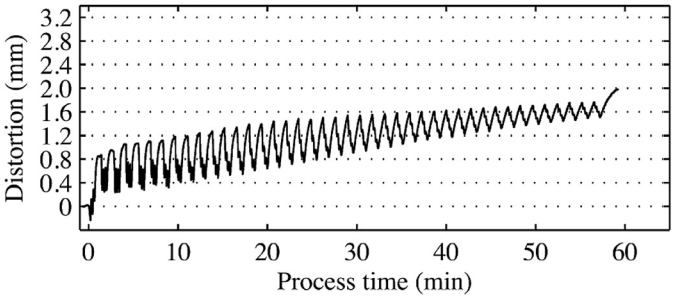

Fig. 5. A distortion history for wall builds by LMD [51].

upward distortion with a cycle of downward-upward displacement during the laser melting and cooling process, as shown in Fig. 5.

2.3. The influencing factors of distortion

Researchers have attempted to explore the influencing factors on the distortion of the AM parts. These factors can be broadly categorized into the following three aspects: Material property, processing, and structure geometry.

The relationship between the distortion and material property has been identified. Mukherjee et al. [60] stated that alloys with lower heat capacity and higher thermal diffusivity often showed higher thermal strain. Yakout et al. [61] reported that materials with lower thermal expansion coefficients, such as Invar 36, exhibited less distortion than those with higher thermal expansion coefficients. Dunbar et al. [49] observed that Inconel 718 parts distorted 80.9% more than Ti6Al4V for the AM parts with the same geometry built by the same machine. Denlinger et al. found that distortion of Inconel 625 part was at least twice than the Ti6Al4V part under the same heat input. This phenomenon might be due to the different phase transformation of deposited materials [51]. The importance of solid-state phase transformation in the numerical prediction of distortion in SLM was also pointed out in Refs. [62,63]. For the FDM process, thermal contractions were found to determine the level of deformation for the amorphous polymers [64]. The distortion of a DLP printed object was caused by the volume shrinkage [65], which depended on the DoC (degree of conversion) of material and stiffness of structure [66]. It can be concluded that the distortion is related to the material property that affects the shrinkage of material, including thermal expansion coefficient, phase transformation, and degree of conversion.

From the perspective of processing, Wu et al. [54] observed that the distortion of prism structure decreased with the increasing energy density. The distortion of cantilever structure can be increased with the part density, scan speed, and laser power [67]. A decrease in layer height combined with the laser power can also result in lower thermal strain and distortion [60]. Yakout et al. [68] found that the cantilever distortion increased with the laser energy density. Liu et al. [69] observed that with the decreasing layer thickness in FDM, the distortion of PLA thin-plate part increased significantly. In addition, the low nozzle temperature helped to reduce the level of distortion. Overall, the part distortion decreased with the energy density in SLM and nozzle temperature in FDM.

Preheating the substrate has been proven as an effective way to decrease the distortion of AM parts [70–72]. Kruth et al. [73] stated that preheating the base plate helped to reduce the temperature gradient of molten pool, leading to a reduced distortion of the AM part. Dunbar et al. [49] found a reduction in the magnitude of distortion in early deposited layers when subjected to heating from subsequent layers. Buchbinder et al. [74] and Denliger et al. [52] found that the higher preheating temperature resulted in less distortion of the SLM built part. Cao et al. [75] illustrated that the higher the number of preheating passes, the lower the distortion. Besides, the cooling time after each preheat scan had no influence on the final distortion. Increasing the preheat temperature of the bed in FDM was also effective in terms of decreasing the distortion [76].

Scan strategy was also found to play a significant role in altering the distortion of the AM part [77–85]. Huang and Jiang [86] reported that the shorter raster scanning produced less distortion than longer raster scanning in SLA. The distortion can be reduced by almost 50% by reducing the length of the scan vectors from 20 mm to 2.5 mm in SLM. If the parallel scan vectors became layer-wise alternated, the distortion reduction can reach 45% [73]. Dunbar et al. [48] used a parallel scan pattern, leading to 37.6% increase of distortion as compared with that using a rotation scan pattern. Li et al. [87] observed that the horizontal scan pattern produced the biggest deflection along cross-wise direction, while the vertical pattern resulted in the smallest deflection. The same phenomenon was also revealed in light curing resin process [88]. Yang et al. [84] stated that for the thin-walled structure, transverse scan was

beneficial for decreasing the distortion, because transverse constraining force acted on the structure with large stiffness.

Geometry also has a significant impact on the distortion of the AM built part. Zhu et al. [89] found that long section length and thin existing part were detrimental to dimensional accuracy as evidenced by the high level of distortion. Kruth et al. [77] observed that the addition of powder can increase the distortion of substrate compared with that without powder. This was attributed to the increased cross-section of the molten pool. For the cantilever structure, the distortion decreased significantly with the increasing arm thickness [74,90]. The stress relaxation for the disk of 5 mm height was more significant than that of 10 mm counterpart, leading to a higher distortion level for the former [91]. The distortion can be increased after the bridge arch was built, indicating that the distortion can be significantly altered by structure optimization [92]. Cheng et al. [93] attempted to decrease the distortion by optimization the support structure.

3. Residual Stress in AM

Residual stress is that which remains in a body that is stationary and at equilibrium with its surroundings [94]. It should be noted that residual stress (long-range stresses, Type I, varying continuously over a length-scale which is comparable to the macroscopic dimension of a component [94,95]) is often measured at ambient temperature. On the contrary, thermal stress reflects the status of stress at elevated temperatures, which creates difficulty for the measurement techniques. Residual stress, which is usually measured at ambient temperature, results from thermal stress accumulated during the AM processes. Crack occurs when the thermal stress is larger than the tensile strength of the material [42], which could appear during AM process and during the separation from the substrate.

It is worth noting that when the residual stress is concerned, one should bear in mind its distribution, direction, magnitude as well as the constrain conditions of the body's surroundings. Residual stress is developed and altered in nearly every stage of manufacturing processes [43]. The distribution of residual stress will be reconstructed if the constrain condition of the part was removed or changed [90,96].

3.1. The distribution of residual stress

The measurement techniques for residual stresses include hole-drilling method [97,98], contour method [99,100], X-ray diffraction (XRD) [101,102], and neutron diffraction (ND) [103,104]. Based on the measured results, it can be concluded that the residual stress distributions in AM parts can be highly anisotropic and its magnitudes can vary significantly. Previous work showed that residual stress parallel to the laser scan direction, i.e., longitudinal direction was larger than that in transversal and normal directions [90,91,105–107]. Parry et al. [108] and Chen et al. [109] found that the longitudinal stress (X-component of stress) was the highest stress direction due to the presence of the larger thermal gradient parallel to the scan vector (Fig. 6(a)), whereas the Z-component of stress was the lowest (Fig. 6(c)). Transversal residual stresses were highly dependent on geometry owing to the different thermal histories [110]. Sun et al. [111] observed that the magnitude of transversal residual stress in the WAAM components was much smaller than that in the substrate due to the low transverse restraint degree of the beam. Residual stress magnitudes in the longitudinal direction were found to be 1.5–2.5 times the magnitude of transversal stress [112–114]. It was mentioned in Ref. [115] that the in-plane residual stresses were usually larger than the normal stresses. Khouzani et al. [91] reported that the normal residual stresses were negligible for as-built parts. To summarize, the longitudinal residual stress appears to be the major stress component.

Mercelis and Kruth [116] reported that the region characterized by tensile residual stresses appeared near the top surface, followed by a zone of compressive stresses, and then changing back to tensile stresses at the bottom. Brown et al. [117] and Liu et al. [118] contoured the residual stress distribution of SLM part by ND technique and numerical simulation, respectively. As shown in Figs. 7 and 8, the longitudinal residual stresses of the SLM part after removal from the substrate showed a characteristic profile of "tensile-compressive-tensile" from the top to bottom of the part. The similar residual stress distribution of "tensile-compressive-tensile" as revealed in AM part was found in many studies involving the AM techniques of SLM, LMD and WAAM [62,119–124]. Such a residual stress profile in AM part is as expected due to the self-equilibrating nature of Type I residual stress over the length-scale of a component. This is consistent with what has been measured in the fusion welding component by using ND technique [104].

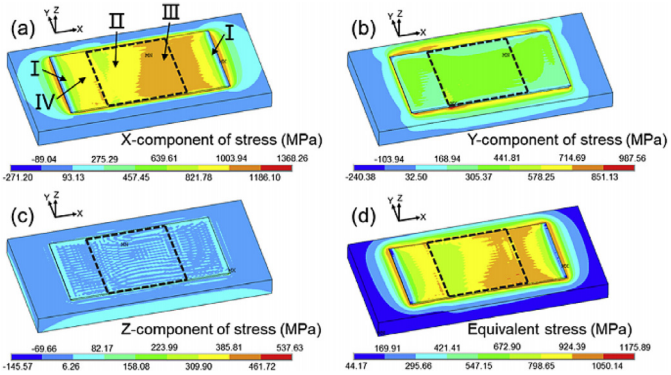

Fig. 6. Residual stress distribution of SLM part at room temperature: (a) *X*-component of stress; (b) *Y*-component of stress; (c) *Z*-component of stress; (d) EQUIVALENT stress [109].

3.2. The evolution of residual stress

Similar to the evolution of distortion in AM, the stress sign of newly added layer was found to change from compressive to tensile during the laser heating and cooling steps [43,73]. As shown in Fig. 9(a), when a new layer is added and heated, this new layer of material will expand initially. However, this expansion is restricted by the underlying part with lower temperature, resulting in the presence of compressive stresses in the new layer while tensile stresses in the underlying part. When the heat source is removed, the new layer will cool down quickly, contracting at a greater rate than the part beneath can accommodate. This is responsible for the presence of tensile stresses in the new layer while compressive stresses in the underlying part, as shown in Fig. 9(b). To satisfy the moment equilibrium, a tensile stress zone is created at the bottom of part [73], forming a stress distribution of "tensile-compressive-tensile" from the top to bottom.

With the layer-by-layer deposition, the longitudinal stress distribution of "tensile-compressive-tensile" from top to bottom of the AM part is well defined. Zhao et al. [125] found that residual stress generated by adding the last layer of LMD always created the tensile sign. The largest tensile stress in the top layer of AM part was confirmed by other researchers as well [44,60,126,127]. In addition, the maximum value of the longitudinal stress was equal to or slightly larger [118,128] than the yield strength of deposited material. It is interesting to note that with deposition of new layers, the tensile stress in the previously deposited layers converted into compressive sign [106]. Mukherjee et al. [129] performed numerical simulation and results showed the tensile stress formed at the top of the AM part after deposited 2 layers. However, the tensile stress at the second layer (Fig. 10(a)) was changed into compressive after depositing 10 layers (Fig. 10(b)). In addition, the wall corners exhibited remarkable stress concentration.

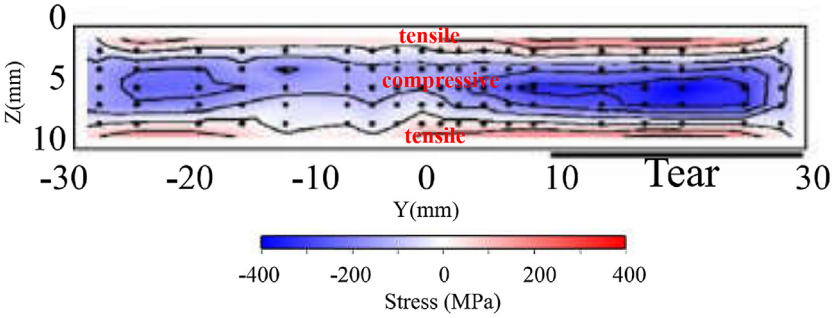

Fig. 7. Neutron diffraction measured distribution of longitudinal residual stress through thickness of a SLM part [117].

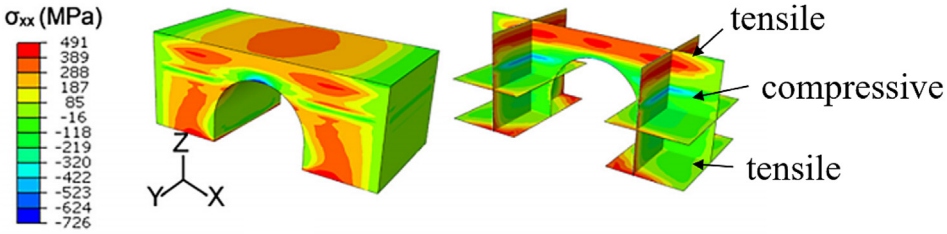

Fig. 8. Numerical simulation predicted longitudinal stress distribution in a SLM part [118].

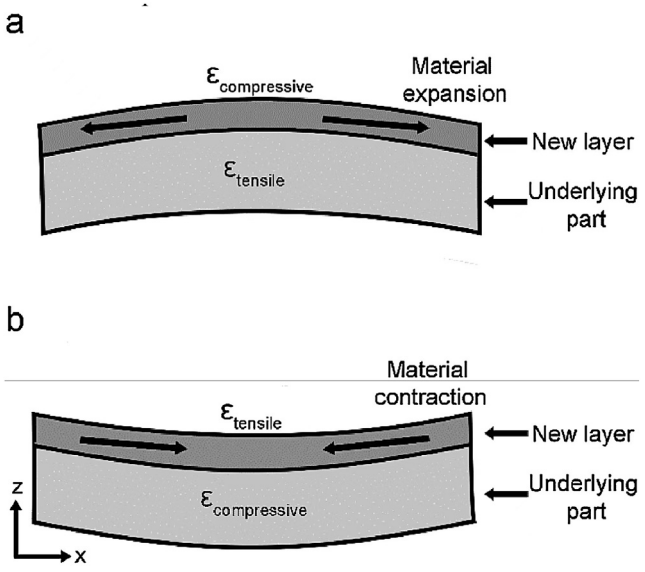

Fig. 9. Basic mechanisms of stress and plastic deformation development during AM: (a) During heating and thermal expansion of the new layer; (b) During cooling and thermal contraction of the new layer [43].

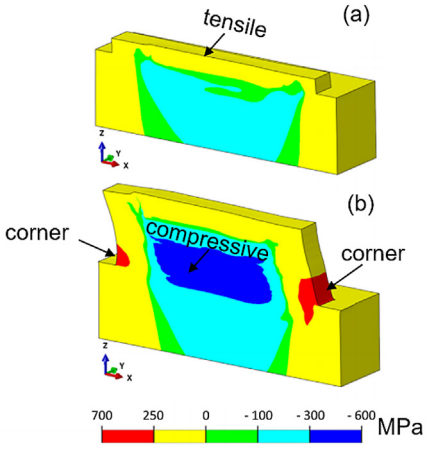

Fig. 10. Numerical simulation predicted residual stress development during the additive process: (a) After the finish of the 2nd layer; (b) After the finish of the 10th layer [129].

3.3. *The influencing factors of residual stress*

The mechanism of residual stress formation in additive processes is driven by the non-uniform material expansion/contraction. Therefore, the thermal and mechanical properties of the material being processed would naturally influence the magnitude of residual stress. The magnitude of residual stress was found to decrease with the increase of thermal diffusivity and thermal conductivity, and the increase of the yield strength [43]. Invar 36 has a much lower coefficient of thermal expansion than 316 L stainless steel and Ti6Al4V, which resulted in the lowest thermal stresses and thus residual stresses [61]. The strain associated with a certain solid-state phase transformation was reported to counteract the thermal stresses and thus greatly reduced final residual stress magnitude [62]. Bailey et al. [130] found that the compressive stresses near the surface in LMD were primarily caused by phase transformation related strains of the H13 tool steel. The residual stress generated in the FDM printed part was significantly influenced by the semi-crystalline physics and the temperature dependent thermo-mechanical properties of the polymer [131]. In this sense, residual stress is related to thermal properties and phase transformation of material.

Studies have attempted to explore the relationship between residual stress and processing parameters. Liu et al. [106] found that the lower energy input and shorter length of scan line can induce smaller residual stress in SLM parts. Simson et al. [132] reported significantly higher residual stress in 316 L stainless steel produced by SLM, when the volumetric energy input was increased. The residual stress decreased with the increase of layer thickness in SLM, because of the decreased temperature gradient [133,134]. Likewise, a considerable reduction in distortion was observed with the increasing layer thickness [135]. Levkulich et al. [136] found that the longitudinal stress on the top surface of the SLM deposit was decreased by increasing laser power, decreasing scan speed, reducing substrate overhang, and decreasing build area. Parry et al. [110] stated that overheating may cause the increased residual stresses. Overall, it can be concluded that the magnitude of residual stress decreases with the decrease of heat input and the increase of layer thickness.

In addition, Shiomi et al. [126] revealed that preheating the base plate to 160 °C helped reducing the residual stress by 40%. A residual stress reduction of 90% was realized in 316 L stainless steel bridge structures by in-situ diode annealing [137]. The thermal stress induced cracks can be avoided by preheating the specimen [138]. Aggarangsi et al. [139] applied a uniform preheat to the deposition surface, which led to a significant change in temperature distribution and residual stress profile.

Scan strategy was reported to have a significant impact on the tensile stress in SLM [108,132,140–143]. Reducing scan vectors and rotating scan vectors were claimed to be beneficial in reducing the residual stress [144, 145]. Parry et al. [110] and Chen et al. [109] stated that longitudinal stress increased with the length of scan lines. Ali et al. [146] investigated the chessboard scanning and results showed that an increasing trend in residual stress with the increased chessboard block size (i.e. scan vector length). A decrease in tensile residual stresses was observed for specimens built using the 3×3 mm^2 island strategy, when compared to the 5×5 mm^2 island counterpart [54]. The tensile stress can be decreased with overlap ratio when it is less than 50% [109]. Upon the reduction of hatch distance from 100 μm to 40 μm, the subsurface residual stress was found to decrease from 600 MPa to 150 MPa [147]. The maximum tensile residual stresses arose in the remelting region [148], but the tensile stresses can be decreased with multiple remelting [149,150].

Colombo et al. [151] demonstrated that the residual stresses of AlSi10Mg samples can be completely relieved by applying the post-processing heat treatments. The residual stress of pure iron sample built by SLM can be eliminated by vacuum heat treatment [152]. Shiomi et al. [126] found that the heat treatment at 600 and 700 °C for one hour was effective to reduce the residual stress by about 70%. Vrancken [145] reported that the stress relief treatment had a noticeable effect on the residual stress and can impact the fatigue crack growth rate.

Studies have been performed to explore the influence of geometry on the residual stress. For rectangular samples, the longitudinal stress distribution of "tensile-compressive-tensile" from top to bottom of the part can be maintained during the layer-by-layer deposition [129,134,153]. The maximum longitudinal residual stress in tension increased from 266 to 609 MPa with the increase of the build height from 2 to 12 mm [154]. However, severe stress concentration can occur at the corners of thin-walled structure [129,155]. For cantilever structure, the tensile stress at the top and the compressive stress at the center of part were also revealed [90,156,157].

4. Mechanism of Distortion and Residual Stress

The shrinkage of material is a common phenomenon in various AM processes. As for the metal AM process, the metal shrinks from liquid to solid. Likewise, the resin contracts during the light curing process. The polymer shrinks from nozzle temperature to bed or room temperature. As an example of the opposite, the part built by selective laser sintering (SLS) process distorted slightly, because the pre-heating temperature was quite close to the glass-transition temperature of the sintered material [56]. The material used in SLS undergoes little contraction, resulting in limited distortion of the built part. It can be concluded that the shrinkage of material is a key cause of distortion and residual stress in various AM processes. This section discusses the formation mechanisms of the distortion and residual stress from both the micro- and macro-scopic perspectives.

4.1. Temperature gradient mechanism

Kruth et al. [73,77,116] proposed the classic temperature gradient mechanism (TGM) to interpret the phenomenon of distortion and residual stresses in SLM; since then, many AM researchers have adopted the idea. The TGM model describes that when the laser beam heats up the added material, it tends to expand as shown in Fig. 11(a). After the laser

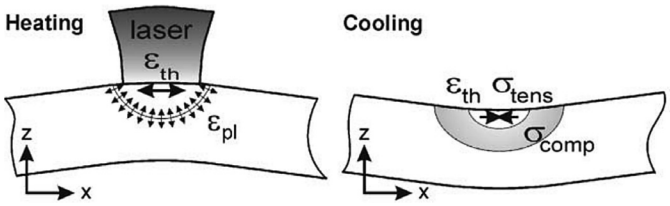

Fig. 11. Schematics of temperature gradient mechanism [75].

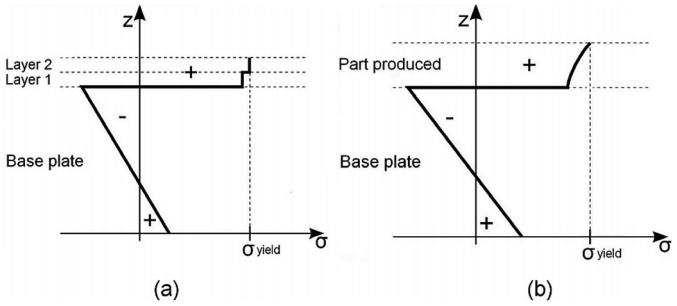

Fig. 12. Schematics of residual stresses formed in SLM part: (a) After adding two layers of melted powders on a base plate; (b) After melting more layers towards the final completion of the built [73].

removes, the temperature of the irradiated zone cools down rapidly, accompanied with the material shrinkage, as shown in Fig. 11(b). However, the shrinkage is partially restricted by the surrounding material, generating a tensile residual stress at the irradiated zone. This explains the presence of high tensile stresses in the initial stage of the SLM process, compressive stresses in the upper part of the base plate, and lower tensile stresses in the lower part of the base plate, as shown in Fig. 12(a). A further powder layer deposition would not change the residual stress profile dramatically, as shown in Fig. 12(b).

The cycle of downward-upward displacement during the laser melting and cooling steps, as well as the "tensile-compressive-tensile" stress distribution from top to bottom of the AM part can be perfectly interpreted by the TGM model. However, some phenomena that cannot be easily explained by the TGM mechanism are worth noting. Some examples are given below: (i) why scan strategy can have a significant effect on the distortion and residual stress; (ii) how does the structural factor influence the distortion, as mentioned in Section 2.3; and (iii) what determines the residual stress concentration as shown in Fig. 10? This opens many opportunities to develop new models so that the level of distortion and residual stresses in AM parts can be better predicted.

4.2. Assumption of constraint force

Xie et al. [56,158] proposed a macro-scopic model that accounted for the material, processing, and structural factors. At the beginning, a cantilever arm was at high temperature, as shown in Fig. 13(a). When it was cooled to ambient temperature, the arm shrunk by u^0 if there was no constraint, as shown in Fig. 13(b). However, the support structure put constraint to the shrinkage of the deposited arm. This resulted in the shrinkage of arm to ${u_1}^s$ rather than u^0, as shown in Fig. 13(c). A couple of constraining forces ${F_1}^s$ can be assumed at the interface between the deposited first layer and the support, see the right schematic diagram of Fig. 13(c). Similarly, a couple of constraining forces ${F_i}^s$ can be assumed at the interface between the deposited layer i and layer i–1.

Xie et al. [56,158] deduced an expression of constraint force at layer N as follows:

$$F_N=k_{ds}\bullet(\alpha_d\bullet\Delta T+\beta_{pt})\bullet E_d\bullet A_d$$

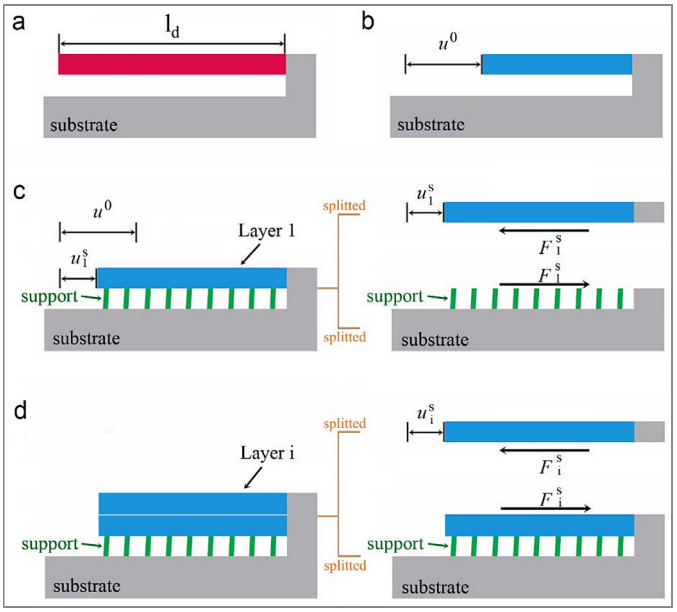

Fig. 13. (a) Assumption of constraint force for deposited arm at high temperature without the support, (b) While at low temperature without the support; (c) Assumption of constraint force between the support and the first layer; (d) Assumption of constraint force between layers of i–1 and i [56].

The defined constraint coefficient k_{ds} reflects the degree of constraint of molten pool. The product of α_d and ΔT depicts the level of thermal shrinkage. β_{pt} is the shrinkage/expansion caused by phase transformation. The α_d is the mean thermal expansion coefficient, while ΔT represents the temperature difference between the solidus temperature and the ambient temperature. E_d and A_d mean the Young's modulus and the cross-section area of the deposited track, respectively.

By assuming a couple of constraint forces between the new deposit and previously deposited layers, the model provided a macro-scopic view to recognize the distortion and residual stress in AM [56,158]. The shrinkage tendency of additive deposition is the intrinsic reason of distortion and residual stress of built parts [52,54,56]. As shown in Fig. 14, each layer has different temporary shrinkage because of the difference of the shear stiffness between the previously deposited structure and the support structure. The inconsistent shrinkage of all layers drives the disengaged part to distort.

The above-mentioned model can be used to help understand the distortion and residual stresses in AM [56]. For example, the preheating can effectively decrease the distortion and residual stresses, because of the decreased temperature difference and the constraint force and shrinkage tendency. In addition, the different scan strategy generates different directions of constraint forces, which cause the different shrinkage and distortion of part. Besides, the structural stiffness and phase transformation of material are important in the discussion of distortion and residual stress in AM, as shown in Fig. 14. This model also reveals the stress distribution of "tensile-compressive-tensile" stress distribution from top to bottom [158]. To summarize, the model of constraint force can be an effective supplement to the TGM model for understanding the distortion and residual stress in AM.

4.3. *Developments of distortion and residual stress*

Residual stress by definition is regarded as purely elastic [43,54]. When the stress surpasses the yield strength, it will cause plastic deformation until the stress is relieved to or below the yield strength. This explains why the maximum longitudinal stress had the magnitude similar to the yield strength of deposited material [118,128]. As a result, the maximum elastic strain and some plastic strain can be assumed at the top of built part (arm), as depicted in Fig. 15(a). After the support is removed, part distortion will occur [41], as shown in Fig. 15(b). The distortion lead to a new distribution of elastic strain (or called residual stress) and plastic strain in the built part. Li et al. [90] found that the residual stress decreased 70% after the support removal. Ding et al. [159] and Khouzani et al. [91] observed significant reduction in the longitudinal stresses after unclamping of the part built by WAAM and SLM, respectively.

The elastic strain can be effectively decreased or eliminated by stress relieving heat treatment [126,145], as shown in Fig. 15(c). The deformation energy of stress relieved part is much less than that of as-built part, leading to a much less distortion of the part after support removal, as shown in Fig. 15(d). Thöne et al. [160] found that after stress relieving treatment (about 800°C for Ti6Al4V), the distortion of cantilevers can be decreased from 0.35 mm to about 0.05 mm. The residual stress (elastic strain) shown in Fig. 15(d) is supposed to be less than that in the part without stress relieving after support removal (shown in Fig. 15(b)).

5. Approaches to Decrease Distortion and Residual Stress

The literature review and analysis lead us to draw the conclusion that the major influencing factors of distortion and residual stress can be classified into three aspects including structure, material, and processing, as shown in Fig. 16. Hence, the approaches to decrease the distortion and residual stress can be illustrated as follows.

5.1. *Pre-processing*

The stiffness of the deposited structure plays an important role in the distortion. The morphology and dimension of deposited structure should be optimized. The part laying angle in the additive process enables variation in the stiffness of the deposited structure, because it can change the slice of the model and the relevant structural stiffness layer-by-layer. In addition, the stiffness of support structure can create significant variations of distortion. The higher stiffness of the support, the less distortion of built part [56].

Geometry compensation may be an effective means to decrease the distortion in AM. Afazov et al. [161] and Seidel and Zaeh [162] simulated the distortion of a blade, and proposed approaches to decrease the distortion by pre-compensation the geometry of the blade. Based on a mass of data about the measured distortion and materials properties, processing, structural stiffness, a data-driven model can be established to make an accurate prediction on the distortion. Following this, the sizes of structure can be modified for compensation before AM process.

To obtain the low distortion and residual stress, the material used is suggested to have low coefficient of thermal expansion. Also, the phase transformation that can generate volume expansion during the cooling process would be useful as it can counteract the thermal shrinkage from high temperature to ambient temperature.

Preheating the substrate is an effective method to reduce the temperature difference between the top and bottom [56], and in turn decreases the distortion and residual stresses of the AM part. It is important to preheat when depositing the first few layers because of their weak structural stiffness. It should also be noted that preheating the platform will result in reduced cooling rates and an increase in grain size, which can reduce mechanical strength of the built part.

5.2. In-situ *processing*

In terms of heat source, laser is deemed to make a smaller heat-affected zone than arc, leading to less distortion than that built by arc. The influence of energy density on distortion seems contradictory, so the primary aim of parameters optimization is to achieve fully densified AM part.

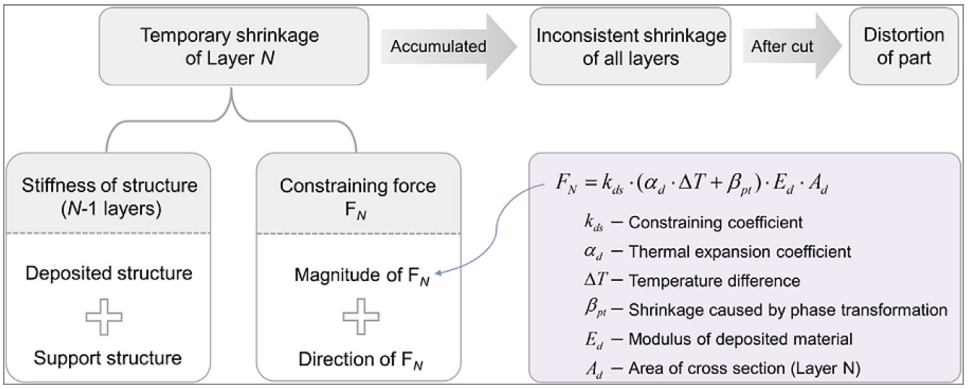

Fig. 14. Mechanism of constraining force induced distortion [56].

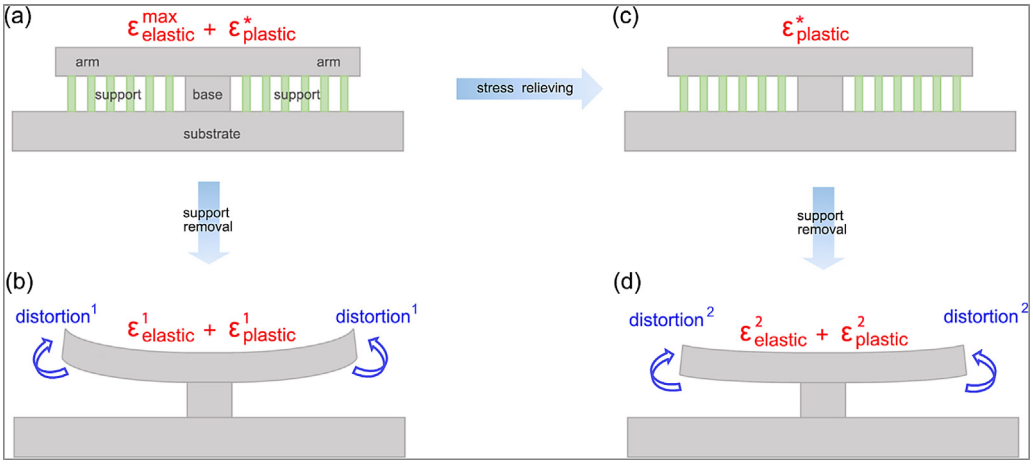

Fig. 15. Schematics of development of distortion and residual stresses: (a) As-built condition; (b) After stress relieving; (c) After support removal without stress relieving; (d) After support removal with stress relieving.

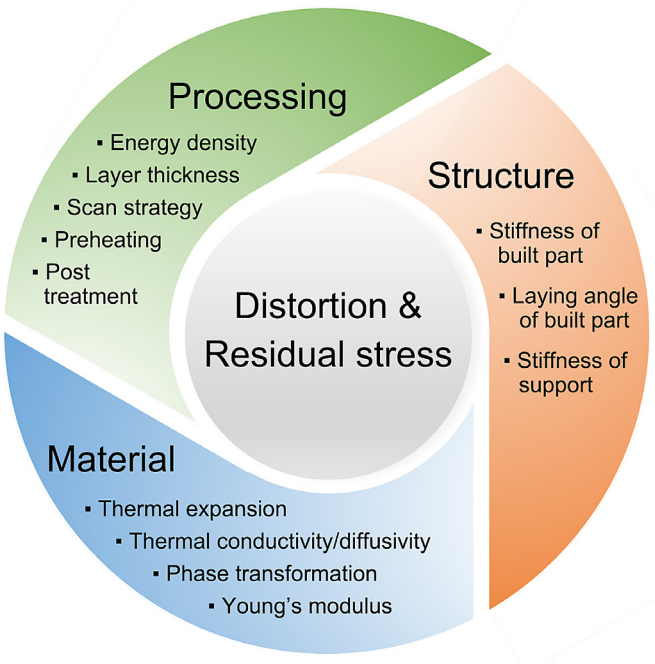

Fig. 16. Influencing factors of distortion and residual stress in AM.

Optimization the scan directions is an effective way to decrease distortion and residual stress. The distortion and residual stress can be viewed as a consequence of constraint forces acting on a structure. The structural stiffness is direction dependent. The laser scan direction can be adjusted in the direction that the structure has the largest shear stiffness. For example, using scan direction perpendicular to the arm of cantilever can cause less distortion than that using scan direction parallel to the arm. Therefore, the scan strategy needs to be optimized in accordance with the structural characterization. A smaller working area of constraint force, a less distortion and tensile stress of the AM built part. The island scan strategy is determined as an effective method to decrease the distortion and residual stress in AM.

5.3. *Post processing*

Post processing for decreasing the distortion and residual stress involves heat treatment and mechanical treatment. Heat treatment has been proven as an effective way to decrease the distortion and residual stresses in AM part. The part is advised to be stress relieved before the support removal, as shown in Fig. 15. It should be noted that the mechanical properties may be worse due to the unwanted grain growth during the heat treatment [163].

Since the tensile stresses are usually generated on the top of built part, it is possible to tailor them by mechanical methods. Laser shock peening (LSP), a surface treatment that can generate compressive stresses, was found to have beneficial effect on modifying the residual stress profile in the part built by SLM [164,165]. It is similar to the concept of shot peening (SP) and ultrasonic shot peening (USP) but uses laser instead. Rolling can decrease the distortion and residual stresses

of the part built by WAAM. The tensile stresses at the top of the AM part can be changed into compressive stresses [122]. The plastic deformation introduced can effectively compensate for the shrinkage of the additive material. Therefore, the LSP, SP, USP, and rolling can be applied for reduction of residual stress and distortion in AM.

6. Conclusions

Distortion and residual stress are two major problems in AM. This work provides an overview towards the mechanisms, evolution, and influencing factors of distortion and residual stresses. Several conclusions can be drawn as follows:

(1) The shrinkage of added deposit that constraint by the previous deposited or surrounding material is the intrinsic cause of distortion and residual stress in AM.
(2) Most of the maximum distortion lie at the far end (or ends) of built part. The longitudinal stresses are distributed as "tensile-compressive-tensile" from top to bottom of built part after cut from the substrate.
(3) The classic temperature gradient mechanism provides a micro perspective towards the evolution of distortion and residual stress. The model of constraining force makes it possible to clarify the influence of structural, material, and processing factors on the distortion and residual stress from a macro perspective.

This work offers a comprehensive understanding of distortion and residual stress, as well as a guideline for decreasing the distortion and residual stress in AM. This work not only advances the discussion towards the distortion and residual stress, but also can improve the success rate of printing and performance of the AM built part.

Declaration of Competing Interest

The authors declare that they have no known competing financial interests or personal relationships that could have influenced the work reported in this paper.

CRediT authorship contribution statement

Deqiao Xie: Drafted the manuscript. **Fei Lv:** Contributed to the reference. **Youwen Yang:** Optimized the structure and figures. **Lida Shen:** Optimized the structure and figures. **Zongjun Tian:** Provided the resources of study and investigation. **Cijun Shuai:** Provided the resources of study and investigation. **Bo Chen:** Carefully revised this manuscript. **Jianfeng Zhao:** Provided the resources of study and investigation.

Acknowledgements

This work was supported by National Key Research and Development Program of China (Grant No. 2018YFB1105400), National Natural Science Foundation of China (Grant No. 51475238), Key Research and Development Program of Jiangsu Provincial Department of Science and Technology of China (Grant No. BE2019002), China Post-Doctoral Fund (Grant No. 2020M671475), UK's Engineering and Physical Sciences Research Council, and EPSRC Early Career Fellowship Scheme [EP/R043973/1].

References

[1] Gu D D, Shi X Y, Poprawe R, et al. Material-structure-performance integrated laser-metal additive manufacturing. Science 2021;372(6545):932.
[2] Meng Z, He J, Li J, et al. Melt-based, solvent-free additive manufacturing of biodegradable polymeric scaffolds with designer microstructures for tailored mechanical/biological properties and clinical applications. Virtual Phys Prototyp 2020;15(4):417–44.
[3] Yang Y, Lu C, Peng S, et al. Laser additive manufacturing of Mg-based composite with improved degradation behavior. Virtual Phys Prototyp 2020;15(1):1–16.
[4] Zhang L, Zhuo L, Tang G, et al. Additive manufacture of metamaterials: a review. J Aeronaut Mater 2018;38(3):10–19.
[5] He R, Zhou N, Zhang K, et al. Progress and challenges towards additive manufacturing of SiC ceramic. J Adv Ceram 2021;10(4):637–74.
[6] ASTM International committee F42 on additive manufacturing technologies ASTM F2792-10 standard terminology for additive manufacturing technologies. West Conshohocken: ASTM; 2009.
[7] Savolainen J, Collan M. How additive manufacturing technology changes business models. Addit Manuf 2020;32:101070.
[8] Attaran M. The rise of 3-D printing: the advantages of additive manufacturing over traditional manufacturing. Bus Horiz 2017;60(5):677–88.
[9] Shuai C, Yang M, Deng F, et al. Forming quality, mechanical properties, and anti-inflammatory activity of additive manufactured Zn-Nd alloy. J Zhejiang Univ Sci A 2020;21(11):876–91.
[10] Maleki E, Bagherifard S, Bandini M, et al. Surface post-treatments for metal additive manufacturing: progress, challenges, and opportunities. Addit Manuf 2021;37:101619.
[11] Adekanye S, Mahamood R, Akinlabi E, et al. Additive manufacturing: the future of manufacturing. Mater Technol 2016;51(5):709–15.
[12] Ghorbani J L, Srivastava A K. Application of optimized laser surface re-melting process on selective laser melted 316L stainless steel inclined parts. J Manuf Process 2020;56:726–34.
[13] Dong D, Chang C, Wang H, et al. Selective laser melting (SLM) of CX stainless steel: theoretical calculation, process optimization and strengthening mechanism. J Mater Sci Technol 2020;73:151–64.
[14] Yan Q, Song B, Shi Y. Comparative study of performance comparison of AlSi10Mg alloy prepared by selective laser melting and casting. J Mater Sci Technol 2020(41):199–208.
[15] Peng P, Yang J, Lee W, et al. Effects of heat treatment of selective laser melting printed Ti-6Al-4V specimens on surface texture parameters and cell attachment. Appl Sci 2021;11:2234.
[16] Williams R, Davies C, Hooper P. A pragmatic part scale model for residual stress and distortion prediction in powder bed fusion. Addit Manuf 2018;22:416–25.
[17] Sing S, An J, Yeong W, et al. Laser and electron-beam powder-bed additive manufacturing of metallic implants: a review on processes, materials and designs. J Orthopaed Res 2016;34(3):369–85.
[18] Mian J, Razmi J, Ladani L. Mechanical behavior of electron beam powder bed fusion additively manufactured Ti6Al4V parts at elevated temperatures. J Manuf Sci Eng 2020;143(2):1–24.
[19] Breuning C, Arnold C, Markl M, et al. A multivariate melt pool stability criterion for fabrication of complex geometries in electron beam powder bed fusion. Addit Manuf 2021;45:102051.
[20] Kruth J P, Mercelis P, Vaerenbergh J V, et al. Binding mechanisms in selective laser sintering and selective laser melting. Rapid Prototyp J 2005;11(1):26–36.
[21] Meng Z, He J, Cai Z, et al. In-situ re-melting and re-solidification treatment of selective laser sintered polycaprolactone lattice scaffolds for improved filament quality and mechanical properties. Biofabrication 2020;12(3):035012.
[22] Qu H P, Li P, Zhang S, et al. Microstructure and mechanical property of laser melting deposition (LMD) Ti/TiAl structural gradient material. Mater Des 2010;31(1):574–82.
[23] Koike R, Misaw T, Kakinuma Y, et al. Basic study on remelting process to enhance density of Inconel 625 in direct energy deposition. Int J Autom Technol 2018;12(3):424–33.
[24] Liu F, Lyu F, Liu F, et al. Laves phase control of Inconel 718 superalloy fabricated by laser direct energy deposition via δ aging and solution treatment. J Mater Res Technol 2020;9(5):9753–65.
[25] Denlinger E R, Michaleris P. Mitigation of distortion in large additive manufacturing parts. Proc Inst Mech Eng Part B J Eng Manuf 2015:983–93.
[26] Yan W, Yue Z, Zhang J. Study on the residual stress and warping of stiffened panel produced by electron beam freeform fabrication. Mater Des 2016;89:1205–12.
[27] Collins P C, Harlow D G. Probability and statistical modeling: Ti-6Al-4V produced via directed energy deposition. J Mater Eng Perform 2021;30(9):6905–12.
[28] Wang Y, Xu X, Zhao Z, et al. Coordinated monitoring and control method of deposited layer width and reinforcement in WAAM process. J Manuf Process 2021;71:306–16.
[29] Geng H, Li J, Xiong J, et al. Geometric limitation and tensile properties of wire and arc additive manufacturing 5A06 aluminum alloy parts. J Mater Eng Perform 2017;26(2):1–9.
[30] Dai Y L, Yu S, Huang A, et al. Microstructure and mechanical properties of high--strength low alloy steel by wire and arc additive manufacturing. Int J Miner Metall Mater 2020;27(7):933–42.
[31] Liu H, Zhao T, Li L, et al. A path planning and sharp corner correction strategy for wire and arc additive manufacturing of solid components with polygonal cross-sections. Int J Adv Manuf Technol 2020;106:1–4.
[32] Eswaran P, Subramaniyan M, Appusamy A, et al. Investigations on acute angle parts fabricated fusion deposition modelling parts volumetric shrinkage and surface roughness. Mater Today Proc 2020;45(2):930–5.
[33] Sood A K, Ohdar R K, Mahapatra S S. Parametric appraisal of mechanical property of fused deposition modelling processed parts. Mater Des 2010;31(1):287–95.
[34] Mukhtarkhanov M, Perveen A, Talamona D. Application of stereolithography based 3D printing technology in investment casting. Micromachines 2020;11(10):946.
[35] Zou Z W, Ye X C. The progress and application of rapid prototying technology. Appl Mech Mater 2015;697:340–3.
[36] Dean D, Fisher J P. Continuous digital light processing (cDLP): highly accurate additive manufacturing of tissue engineered bone scaffolds. Virtual Phys Prototyp 2012;7(1):13–24.
[37] Kim S H, Ueon Y Y, Lee J, et al. Precisely printable and biocompatible silk fibroin bioink for digital light processing 3D printing. Nat Commun 2018;9(1):1620.

[38] Wallace J, Wang M, Thompson P, et al. Validating continuous digital light processing (cDLP) additive manufacturing accuracy and tissue engineering utility of a dye-initiator package. Biofabrication 2014;6(1):015003.
[39] Jiao C, Gu J, Cao Y, et al. Preparation of Al_2O_3-ZrO_2 scaffolds with controllable multi-level pores via digital light processing. J Eur Ceram Soc 2020;40(15):6087–94.
[40] Wang K, Qiu M, Jiao C, et al. Study on defect-free debinding green body of ceramic formed by DLP technology. Ceram Int 2019;46(2):2438–46.
[41] Anandan K H, Kumaraguru S. Distortion in metal additive manufactured parts, 3D printing and additive manufacturing technologies. Singapore: Springer; 2019.
[42] Li Q, Zhang H, Li D, et al. Comparative study of the microstructures and mechanical properties of laser metal deposited and vacuum arc melted refractory NbMoTa medium entropy alloy. Int J Refract Met Hard Mater 2020;88:105195.
[43] Bartlett J L, Li X. An overview of residual stresses in metal powder bed fusion. Addit Manuf 2019;27:131–49.
[44] Li C, Liu Z, Fang X, et al. Residual stress in metal additive manufacturing. Procedia CIRP 2018;71:348–53.
[45] Fang Z, Wu Z, Huang C, et al. Review on residual stress in selective laser melting additive manufacturing of alloy parts. Opt Laser Technol 2020;129:106283.
[46] Marimuthu S, Clark D, Allen J, et al. Finite element modelling of substrate thermal distortion in direct laser additive manufacture of an aero-engine component. Proc Inst Mech Eng Part C J Mech Eng Sci 2012;227(9):1987–99.
[47] Ghnatios C, Rai K, Hascoet N, et al. Reduced order modeling of selective laser melting: from calibration to parametric part distortion. Int J Mater Form 2021;14:973–86.
[48] Dunbar A J, Denlinger E R, Heigel J, et al. Development of experimental method for *in situ* distortion and temperature measurements during the laser powder bed fusion additive manufacturing process. Addit Manuf 2016;12:25–30.
[49] Dunbar A J, Denlinger E R, Gouge M F, et al. Comparisons of laser powder bed fusion additive manufacturing builds through experimental *in situ* distortion and temperature measurements. Addit Manuf 2017;15:57–65.
[50] Denlinger E R, Gouge M, Irwin J, et al. Thermomechanical model development and *in situ* experimental validation of the laser powder-bed fusion process. Addit Manuf 2017;16:73–80.
[51] Denlinger E R, Heigel J C, Michaleris P, et al. Effect of inter-layer dwell time on distortion and residual stress in additive manufacturing of titanium and nickel alloys. J Mater Process Technol 2015;215:123–31.
[52] Denlinger E R, Heigel J C, Michaleris P. Residual stress and distortion modeling of electron beam direct manufacturing Ti-6Al-4V. Proc Inst Mech Eng Part B J Eng Manuf 2015;229(10):1803–13.
[53] Biegler M, Graf B, Rethmeier M. In-situ distortions in LMD additive manufacturing walls can be measured with digital image correlation and predicted using numerical simulations. Addit Manuf 2018;20:101–10.
[54] Wu A, Brown S, Donald W, et al. An experimental investigation into additive manufacturing-induced residual stresses in 316L stainless steel. Metall Mater Trans A 2014;45(13):6260–70.
[55] Montevecchi F, Venturini G, Grossi N, et al. Finite element mesh coarsening for effective distortion prediction in wire arc additive manufacturing. Addit Manuf 2017;18:145–55.
[56] Xie D, Lv F, Zhao J, et al. Towards a comprehensive understanding of distortion in additive manufacturing based on assumption of constraining force. Virtual Phys Prototyp 2021;16:85–97.
[57] Prabhakar P, Sames W, Dehoff R, et al. Computational modeling of residual stress formation during the electron beam melting process for Inconel 718. Addit Manuf 2015;7:83–91.
[58] Zhang Y, Zhang J. Finite element simulation and experimental validation of distortion and cracking failure phenomena in direct metal laser sintering fabricated component. Addit Manuf 2017;16:49–57.
[59] Wen Y, Zhang B, Liu S, et al. A novel experimental method for *in situ* strain measurement during selective laser melting. Virtual Phys Prototyp 2020;15(s1):83–95.
[60] Mukherjee T, Manvatkar V, De A, et al. Mitigation of thermal distortion during additive manufacturing. Scr Mater 2017;127:79–83.
[61] Yakout M, Elbestawi M, Veldhuis S C, et al. Influence of thermal properties on residual stresses in SLM of aerospace alloys. Rapid Prototyp J 2020;26:213–22.
[62] Denlinger E R, Michaleris P. Effect of stress relaxation on distortion in additive manufacturing process modeling. Addit Manuf 2016;12:51–9.
[63] Tan P, Shen F, Li B, et al. A thermo-metallurgical-mechanical model for selective laser melting of Ti6Al4V. Mater Des 2019;168:107642.
[64] Armillotta A, Bellotti M, Cavallaro M. Warpage of FDM parts: experimental tests and analytic model. Robot Comput Integr Manuf 2018;50:140–52.
[65] Qiang Z, Weng S, Hamel C, et al. Design for the reduction of volume shrinkage-induced distortion in digital light processing 3d printing. Extreme Mech Lett 2021;48:101403.
[66] Wu D, Zhao Z, Zhang Q, et al. Mechanics of shape distortion of DLP 3D printed structures during UV post-curing. Soft Matter 2019;15:6151.
[67] Mugwagwa L, Dimitrov D, Matope S, et al. Influence of process parameters on residual stress related distortions in selective laser melting. Procedia Manuf 2018;21:92–99.
[68] Yakout M, Elbestawi M A, Veldhuis S C. A study of the relationship between thermal expansion and residual stresses in selective laser melting of Ti-6Al-4V. J Manuf Process 2020;52:181–92.
[69] Liu X, Li S, Liu Z, et al. An investigation on distortion of PLA thin-plate part in the FDM process. Int J Adv Manuf Technol 2015;79:1117–26.
[70] Zaeh M F, Brannen G. Investigations on residual stresses and deformations in selective laser melting. Prod Eng 2020;4:35–45.
[71] Colin T C, Bartovt J. As fabricated and heat-treated microstructures of the Ti-6AI-4V alloy processed by selective laser melting. Metall Mater Trans A Phys Metall Mater Sci 2011;42:3190–9.
[72] Zhang K, Wang S, Liu W, et al. Effects of substrate preheating on the thin-wall part built by laser metal deposition shaping. Appl Surf Sci 2014;317:839–55.
[73] Kruth J P, Deckers J, Yasa E, et al. Assessing and comparing influencing factors of residual stresses in selective laser melting using a novel analysis method. Proc Inst Mech Eng Part B J Eng Manuf 2012;226(6):980–91.
[74] Buchbinder D, Meiners W, Pirch N, et al. Investigation on reducing distortion by preheating during manufacture of aluminum components using selective laser melting. J Laser Appl 2014;26(1):012004.
[75] Cao J, Gharghouri M A, Nash P. Finite-element analysis and experimental validation of thermal residual stress and distortion in electron beam additive manufactured Ti-6Al-4V build plates. J Mater Process Technol 2016;237:409–19.
[76] Rosli A A, Shuib R K, Ishak K, et al. Influence of bed temperature on warpage, shrinkage and density of various acrylonitrile butadiene styrene (ABS) parts from fused deposition modelling. AIP Conf Proc 2020;2267(1):020072.
[77] Kruth J P, Froyen L, Van Vaerenbergh J, et al. Selective laser melting of iron-based powder. J Mater Process Technol 2004;149(1–3):616–22.
[78] Ming G, Wang Z, Li X, et al. The effect of deposition patterns on the deformation of substrates during direct laser fabrication. J Eng Mater Technol 2013;135(3):034502.
[79] Nickel A H, Barnett D M, Prinz F B. Thermal stresses and deposition patterns in layered manufacturing. Mater Sci Eng A 1999;317(1–2):59–64.
[80] Hui Y, Shen L, Wang X, et al. Stress and deformation evaluation of the subarea scanning effect in direct laser-deposited Ti-6Al-4V. Int J Adv Manuf Technol 2018;97:1–4.
[81] Dai K, Shaw L. Distortion minimization of laser-processed components through control of laser scanning patterns. Rapid Prototyp J 2002;8:270–6.
[82] Liu W, Saleheen K, Tang Z, et al. Review on scanning pattern evaluation in laser-based additive manufacturing. Opt Eng 2021;60(7):070901.
[83] Lu X, Chiumenti M, Cervera M, et al. Warpage analysis and control of thin-walled structures manufactured by laser powder bed fusion. Metals 2021;11(5):686 (Basel).
[84] Yang T, Xie D, Yue W, et al. Distortion of thin-walled structure fabricated by selective laser melting based on assumption of constraining force-induced distortion. Metals 2019;9:1281 (Basel).
[85] Huang Y, Jiang C. Curl distortion analysis during photopolymerisation of stereolithography using dynamic finite element method. Int J Adv Manuf Technol 2003;21:586–95.
[86] Salem M, Roux S, Hor A, et al. A new insight on the analysis of residual stresses related distortions in selective laser melting of Ti-6Al-4V using the improved bridge curvature method. Addit Manuf 2020;36:101586.
[87] Li C, Fu C, Guo Y, et al. Fast prediction and validation of part distortion in selective laser melting. Procedia Manuf 2015;1:355–65.
[88] Khoshkhoo A, Carrano A L, Blersch D M. Effect of build orientation and part thickness on dimensional distortion in material jetting processes. Rapid Prototyp J 2018;24(9):1563–71.
[89] Zhu Z, Dhokia V, Nassehi A, et al. Investigation of part distortions as a result of hybrid manufacturing. Robot Comput Integr Manuf 2016;37:23–32.
[90] Li C, Liu J F, Fang X Y, et al. Efficient predictive model of part distortion and residual stress in selective laser melting. Addit Manuf 2017;17:157–68.
[91] Khouzani M G, Peng M, Rogge H, et al. Experimental measurement of residual stress and distortion in additively manufactured stainless steel components with various dimensions. Mater Sci Eng A 2017;707:689–700.
[92] Zielinski J, Mindt H, Düchting J, et al. Numerical and experimental study of Ti6Al4V components manufactured using powder bed fusion additive manufacturing. JOM 2017;69(12):2711–18.
[93] Cheng L, Liang X, Bai J, et al. On utilizing topology optimization to design support structure to prevent residual stress induced build failure in laser powder bed metal additive manufacturing. Addit Manuf 2019;27:290–304.
[94] Withers P J, Bhadeshia H. Residual stress - II: nature & origins. Mater Sci Technol 2001;17:366–75.
[95] Chen B, Flewitt P E J, Cocks A, et al. A review of the changes of internal state related to high temperature creep of polycrystalline metals and alloys. Intl Mater Rev 2015;60(1):1–29.
[96] Honnige J R, Colegrove P A, Ahmed B, et al. Residual stress and texture control in Ti-6Al-4V wire+arc additively manufactured intersections by stress relief and rolling. Mater Des 2018;150:193–205.
[97] Vangi D. Residual stress evaluation by the hole-drilling method with off-center hole: an extension of the integral method. J Eng Mater Technol 1997;119:79–85.
[98] Flaman M T, Manning B H. Determination of residual-stress variation with depth by the hole-drilling method. Exp Mech 1985;25(3):205–7.
[99] Pagliaro P, Prime M, Swenson H, et al. Measuring multiple residual stress components using contour method and multiple cuts. Exp Mech 2010;50(187):187–94.
[100] Prime M B. Cross-sectional mapping of residual stresses by measuring the surface contour after a cut. J Eng Mater Technol 2001;123:162–8.
[101] Fitzpatrick M E. Determination of residual stresses by X-ray diffraction: issue 2. Teddington: National Physical Laboratory; 2005.
[102] Prevey P S. X-Ray diffraction residual stress techniques. Metals handbook. American Society for Metals; 1986. p. 380–92.
[103] Goel S, Neikter M, Capek J, et al. Residual stress determination by neutron diffraction in powder bed fusion-built Alloy 718: influence of process parameters and post-treatment. Mater Des 2020;195:109045.
[104] Chen B, Skouras A, Wang Y Q, et al. *In situ* neutron diffraction measurement of residual stress relaxation in a welded steel pipe during heat treatment. Mater Sci Eng A 2014;590:374–83.

[105] Allen A, Hutchings M, Windsor C, et al. Neutron diffraction methods for the study of residual stress fields. Adv Phys 1985;34(4):445–73.
[106] Liu Y, Yang Y, Wang D. A study on the residual stress during selective laser melting (SLM) of metallic powder. Int J Adv Manuf Technol 2016;87:647–56.
[107] Chen C, Yin J, Zhu H, et al. The effect of process parameters on the residual stress of selective laser melted Inconel 718 thin-walled part. Rapid Prototyp J 2019;25(8):1359–69.
[108] Parry L, Ashcroft I A, Wildman R D. Understanding the effect of laser scan strategy on residual stress in selective laser melting through thermo-mechanical simulation. Addit Manuf 2016;12:1–15.
[109] Chen C, Yin J, Zhu H, et al. Effect of overlap rate and pattern on residual stress in selective laser melting. Int J Mach Tools Manuf 2019;145:103433.
[110] Parry L, Ashcroft I A, Wildman R D. Geometrical effects on residual stress in selective laser melting. Addit Manuf 2018;25:166–75.
[111] Sun J, Hensel J, Khler M, et al. Residual stress in wire and arc additive manufactured aluminum components. J Manuf Process 2021;65(5):97–111.
[112] Yadroitsava I, Grewar S, Hattingh D, et al. Residual stress in SLM Ti6Al4V alloy specimens. Mater Sci Forum 2015(828–829):305–10.
[113] Gusaroy A V, Pavlov M, Smurov I. Residual stresses at laser surface remelting and additive manufacturing. Phys Procedia 2011;12:248–54.
[114] Robinson J, Ashton I, Fox P, et al. Determination of the effect of scan strategy on residual stress in laser powder bed fusion additive manufacturing. Addit Manuf 2018;25:13–24.
[115] Hussein A, Hao L, Yan C, et al. Finite element simulation of the temperature and stress fields in single lavers built without-support in selective laser melting. Mater Des 2013;52:638–47.
[116] Mercelis P, Kruth J P. Residual stresses in selective laser sintering and selective laser melting. Rapid Prototyp J 2006;2(5):254–65.
[117] Brown D W, Bernardin J D, Carpenter J, et al. Neutron diffraction measurements of residual stress in additively manufactured stainless steel. Mater Sci Eng A 2016;678:291–8.
[118] Liu C, Fang Z, Guo X, et al. On the simulation scalability of predicting residual stress and distortion in selective laser melting. J Manuf Sci Eng Trans ASME 2018;140(4):041013.
[119] Wang Z, Denlinger E, Michaleris P, et al. Residual stress mapping in Inconel 625 fabricated through additive manufacturing: method for neutron diffraction measurements to validate thermomechanical model predictions. Mater Des 2016;113:169–77.
[120] Hodge N E, Ferencz R M, Vignes R M. Experimental comparison of residual stresses for a thermomechanical model for the simulation of selective laser melting. Addit Manuf 2016;12:159–68.
[121] Szost A, Terzi S, Martina M, et al. A comparative study of additive manufacturing techniques: Residual stress and microstructural analysis of CLAD and WAAM printed Ti6Al4V components. Mater Des 2016;89:559–67.
[122] Martina F, Roy M J, Szost B A, et al. Residual stress of as-deposited and rolled wire+arc additive manufacturing Ti6Al4V components. Mater Sci Technol 2016;32(14):1439–48.
[123] Suárez A, Amado J M, Tobar M J, et al. Study of residual stresses generated inside laser cladded plates using FEM and diffraction of synchrotron radiation. Surf Coat Technol 2010;204(12–13):1983–8.
[124] Moat R J, Pinkerton A J, Li L, et al. Residual stresses in laser direct metal deposited Waspaloy. Mater Sci Eng A 2011;528(6):2288–98.
[125] Zhao X, Iyer A, Promoppatum P, et al. Numerical modeling of the thermal behavior and residual stress in the direct metal laser sintering process of titanium alloy products. Addit Manuf 2017;14:126–36.
[126] Shiomi M, Osakada K, Nakamura K, et al. Residual stress within metallic model made by selective laser melting process. CIRP Ann Manuf Technol 2004;53:195–8.
[127] Strantza M, Vrancken B, Prime M B, et al. Directional and oscillating residual stress on the mesoscale in additively manufactured Ti-6Al-4V. Acta Mater 2019;168:299–308.
[128] Turichin G, Zemlyakov E, Babkin K, et al. Analysis of distortion during laser metal deposition of large parts. Procedia CIRP 2018;74:154–7.
[129] Mukherjee T, Zuback J, Zhang W, et al. Residual stresses and distortion in additively manufactured compositionally graded and dissimilar joints. Comput Mater Sci 2017;143:325–37.
[130] Bailey N S, Katinas C, Shin Y C. Laser direct deposition of AISI H13 tool steel powder with numerical modeling of solid phase transformation, hardness, and residual stresses. J Mater Process Technol 2017;247:223–33.
[131] Samy A A, Golbang A, Jones E, et al. Prediction of part distortion in fused deposition modelling (FDM) of semi-crystalline polymers via comsol: Effect of printing conditions. CIRP J Manuf Sci Technol 2021;33:443–53.
[132] Simson T, Emmel A, Dwars A, et al. Residual stress measurements on AISI 316L samples manufactured by selective laser melting. Addit Manuf 2017;17:183–9.
[133] Ke L, Yin J, Zhu H, et al. Numerical simulation of stress evolution of thin-wall titanium parts fabricated by selective laser melting. Acta Metall Sin 2020;56(3):374–384.
[134] Anderson L S, Venter A M, Vrancken B, et al. Investigating the residual stress distribution in selective laser melting produced Ti-6Al-4V using neutron diffraction. Meca Sens 2018;4:73–8.
[135] Zaeh M F, Branner G. Investigations on residual stresses and deformations in selective laser melting. Prod Eng 2010;4:35–45.
[136] Levkulich N C, Semiatin S L, Gockel J E, et al. The effect of process parameters on residual stress evolution and distortion in the laser powder bed fusion of Ti-6Al-4V. Addit Manuf 2019;28:475–84.
[137] Roehling J D, Smith W, Roehling T, et al. Reducing residual stress by selective large-area diode surface heating during laser powder bed fusion additive manufacturing. Addit Manuf 2019;28:228–35.
[138] Labudovic M, Hu D, Kovacevic R. A three dimensional model for direct laser metal powder deposition and rapid prototyping. J Mater Sci 2003;38(1):35–49.
[139] Aggarangsi P, Beuth J L. Localized preheating approaches for reducing residual stress in additive manufacturing. In: Proceedings of the international solid freeform fabrication symposium; 2006. p. 709–20.
[140] Li C, Fu C, Guo B, et al. A multiscale modeling approach for fast prediction of part distortion in selective laser melting. J Mater Process Technol 2016;229:703–12.
[141] Cheng B, Shrestha S, Chou K. Stress and deformation evaluations of scanning strategy effect in selective laser melting. Addit Manuf 2016;12:240–51.
[142] SomasheKara M A, Naveenkumar M, Kumar A, et al. Investigations into effect of weld-deposition pattern on residual stress evolution for metallic additive manufacturing. Int J Adv Manuf Technol 2017;90:2009–25.
[143] Robinson J, Ashton I, Fox P, et al. Determination of the effect of scan strategy on residual stress in laser powder bed fusion additive manufacturing. Addit Manuf 2018;23:13–24.
[144] Lu Y, Wu S, Yan Y, et al. Study on the microstructure, mechanical property and residual stress of SLM Inconel-718 alloy manufactured by differing island scanning strategy. Opt Laser Technol 2015;75:197–206.
[145] Vrancken B. Study of residual stresses in selective laser melting. Leuven: Catholic University of Leuven; 2016.
[146] Ali H, Ghadbeigi H, Mumtaz K. Effect of scanning strategies on residual stress and mechanical properties of selective laser melted Ti6Al4V. Mater Sci Eng A 2018;712:175–87.
[147] Mishurova T, Artzt K, Haubrich J, et al. New aspects about the search for the most relevant parameters optimizing SLM materials. Addit Manuf 2019;25:325–34.
[148] Gusarov A V, Pavlov M, Smurov I. Residual stresses at laser surface remelting and additive manufacturing. In: Proceedings of the international WLT conference on lasers in manufacturing, 12; 2011. p. 248–54.
[149] Wei K, Lv M, Zheng X, et al. Effect of laser remelting on deposition quality, residual stress, microstructure, and mechanical property of selective laser melting processed Ti-5Al-2.5 Sn alloy. Mater Charact 2019;150:67–77.
[150] Yu W, Sing S L, Chua C K, et al. Influence of re-melting on surface roughness and porosity of AlSi10Mg parts fabricated by selective laser melting. J Alloys Compd 2019;792:574–81.
[151] Colombo C, Biffi C A, Fiocchi J, et al. Effect of optimized heat treatments on the tensile behavior and residual stresses of selective laser melted AlSi10Mg samples. Key Eng Mater 2019;813:364–9.
[152] Song B, Dong S, Qi L, et al. Vacuum heat treatment of iron parts produced by selective laser melting: microstructure, residual stress and tensile behavior. Mater Des 2014;54(2):727–33.
[153] Wu Q, Mukherjee T, Liu C, et al. Residual stresses and distortion in the patterned printing of titanium and nickel alloys. Addit Manuf 2019;29:100808.
[154] Hou P, Mooraj S, Champagne V, et al. Effect of build height on temperature evolution and thermally induced residual stresses in plasma arc additively manufactured stainless steel. Metall Mater Trans A 2022;53(2):627–39.
[155] Sun J, Hensel J, Khler M, et al. Residual stress in wire and arc additively manufactured aluminum components. J Manuf Process 2021;65(5):97–111.
[156] Li L, Pan T, Zhang X, et al. Deformations and stresses prediction of cantilever structures fabricated by selective laser melting process. Rapid Prototyp J 2021;27(3):453–64.
[157] Olleak A, Xi Z. A study of modeling assumptions and adaptive remeshing for thermomechanical finite element modeling of the LPBF process. Int J Adv Manuf Technol 2021;115(11):3599–615.
[158] Xie D, Zhao J, Liang H, et al. Assumption of constraining force to explain distortion in laser additive manufacturing. Materials 2018;11(11):11112327 (Basel).
[159] Ding J, Colegrove P, Mehnen J, et al. Thermo-mechanical analysis of wire and arc additive layer manufacturing process on large multi-layer parts. Comput Mater Sci 2011;50(12):3315–22.
[160] Thöne M, Leuders S, Riemer A, et al. Influence of heat-treatment on selective laser melting products Ti6Al4V. In: Proceedings of the international solid freeform fabrication symposium, Austin Texas; 2012.
[161] Afazov S, Denmark W, Toralles B, et al. Distortion prediction and compensation in selective laser melting. Addit Manuf 2017;17:15–22.
[162] Seidel C, Zaeh M F. Multi-scale modelling approach for contributing to reduced distortion in parts made by laser-based powder bed fusion. Procedia CIRP 2018;67:197–202.
[163] Jiang X, Xiong W, Wang L, et al. Heat treatment effects on microstructure-residual stress for selective laser melting AlSi10Mg. Mater Sci Technol 2020;36(2):168–80.
[164] Kalentics N, Boillat E, Peyre P, et al. Tailoring residual stress profile of selective laser melted parts by laser shock peening. Addit Manuf 2017;16:90–7.
[165] Kalentics N, Seijas M O, Griffiths S, et al. 3D laser shock peening - a new method for improving fatigue properties of selective laser melted parts. Addit Manuf 2020;33:101112.